

Emergence of dynamical hysteresis in a second-order non-autonomous chaotic circuit *

G. Sivaganesh¹, K. Srinivasan², T. Fonzin Fozin³, and R. Gladwin Pradeep⁴

¹Department of Physics, Alagappa Chettiar Government College of Engineering and Technology, Karaikudi, Tamilnadu-630 003, India

²Department of Physics, Nehru Memorial College, Puthanampatti, Tiruchirapalli, Tamilnadu - 621 007, India (Affiliated to Bharathidasan University, Tiruchirapalli, Tamilnadu - 620 024, India)

³Department of Electrical and Electronic Engineering, Faculty of Engineering and Technology (FET), University of Buea, P.O. Box 63, Buea, Cameroon

⁴Department of Physics, KCG College of Technology, Chennai - 600 097, India

March 7, 2023

Abstract

The observation of hysteresis in the dynamics of a third-order autonomous chaotic system namely, the *Chua's* circuit has been reported recently [1]. In the present work, we report the emergence of dynamical hysteresis in a simple second-order non-autonomous chaotic system. The *Murali-Lakshmanan-Chua* (MLC) circuit is studied for the evolution of hysteresis in its dynamics. Numerical simulation and electronic circuit experimental results are presented for the hysteresis behavior and are validated through explicit analytical solutions. The observation of dynamical hysteresis in second-order non-autonomous systems is reported in the literature for the first time.

1 Introduction

The phenomenon of dynamical hysteresis has been observed in the *Chua's* circuit recently [1]. The *Chua's* circuit being the first electronic circuit to exhibit chaos [2] and the evolution of chaos in the circuit has been extensively studied [3, 4]. The construction of the nonlinear resistor using Op-Amps [5] has instigated the development several chaotic circuit systems. In addition to chaos,

*Preprint to be submitted to Chaos Solitons & Fractals

different dynamical behaviors such as quasiperiodic, hyperchaos, strange non-chaos, intermittency, to mention a few, are observed in the variants of *Chua's* circuit [6–10]. The dynamical behaviors of the *Chua's* circuit and its variants have been studied analytically [11, 12]. The emergence of chaos and hysteresis together in chaotic systems termed as *chaotic hysteresis* has been observed in few systems [13–15]. The rise of mixed mode and bursting oscillations due to the asymmetry induced in *Chua's* circuit by DC offset voltage has been reported [16, 17]. Further, the expansion and contraction of attractors due to DC offset voltage in the *Chua's* circuit and an improved memristive *Chua's* circuit with DC offset exhibiting hidden attractors and asymmetric dynamics has been observed and reported [18, 19]. Recently, the effect of DC offset voltage leading to the emergence of the phenomenon of chaotic hysteresis in the dynamics of the *Chua's* circuit has been observed by Gomes *et al.* [1]. The variation of the DC offset from negative to positive values and *vice-versa* yielding dynamical paths yielding hysteresis in the system dynamics due to the switching of the dynamical regimes between the different planes encompassing the fixed points of the system is observed. The expansion and contraction of the attractors in different dynamical regimes has been observed. Further, the evolution of dynamical hysteresis due to the variation of a triangular voltage source is also reported in the *Chua's* circuit.

A simplest second-order non-autonomous dissipative nonlinear circuit consisting of the *Chua's* diode as the only nonlinear element was introduced by Murali *et al.* [20–22]. This circuit is now known as the MLC circuit exhibiting rich variety of bifurcation, chaos, strange non-chaos and synchronization phenomena has been well studied through electronic circuit experiments, numerical simulations and analytical solutions [22–26]. The multistability behavior of the MLC circuit operating in the one-band chaotic state leading to the application of this dynamical state to perform logic operations have been studied [27]. Further, the several bifurcation phenomena and chaos has been observed in memristor based MLC circuits [28–30]. Analytical solutions for a class of second-order chaotic systems with simple nonlinear functions have been developed [31].

In the present work, we report the emergence of chaotic hysteresis in the dynamics of the MLC circuit upon the addition of an DC offset voltage in the circuit. The variation of the offset voltage factor giving rise to the hysteresis phenomenon in the system dynamics is studied. Electronic circuit experimental results indicating the dynamical hysteresis is validated through numerical and analytical results. This paper is organized as follows. In Sec. 2, the hysteresis phenomenon observed in the MLC circuit studied using experimental phase portraits is presented. In Sec. 3, the numerical simulation results explaining the emergence of hysteresis through bifurcation diagram is presented and in Sec. 4, the analytical solutions developed for the normalized circuit equations to study the hysteresis phenomenon is reported. Finally, the conclusion is given in Sec. 5.

2 Dynamical hysteresis: Experimental results

The circuit realization of the simple non-autonomous (MLC) circuit is shown in Fig. 1. It contains a capacitor, an inductor, a linear resistor, an external periodic forcing and only one nonlinear element, namely, the Chua's diode (N_R). In order to measure the inductor current i_L in our experiments, we insert a small current sensing resistor R_s as shown Fig. 1.

By applying Kirchhoff's laws to this circuit, the governing equations for the voltage v across the capacitor C and the current i_L through the inductor L are represented by the following set of two first-order non-autonomous differential equations as

$$C \frac{dv}{d\tau} = i_L - g(v), \quad (1a)$$

$$L \frac{di_L}{d\tau} = -(R + R_s)i_L - v + F \sin(\Omega\tau) + E, \quad (1b)$$

where $F(t)$ is the sinusoidal periodic force with amplitude F and angular frequency Ω . The term E represents a constant voltage added in addition to the sinusoidal voltage source ($F(t)$) is called as the *DC* offset voltage which can be negative or positive. The value of *DC* offset voltage shifts the signals to the same amount of its value. The term $g(v)$ represents the $v - i$ characteristics of

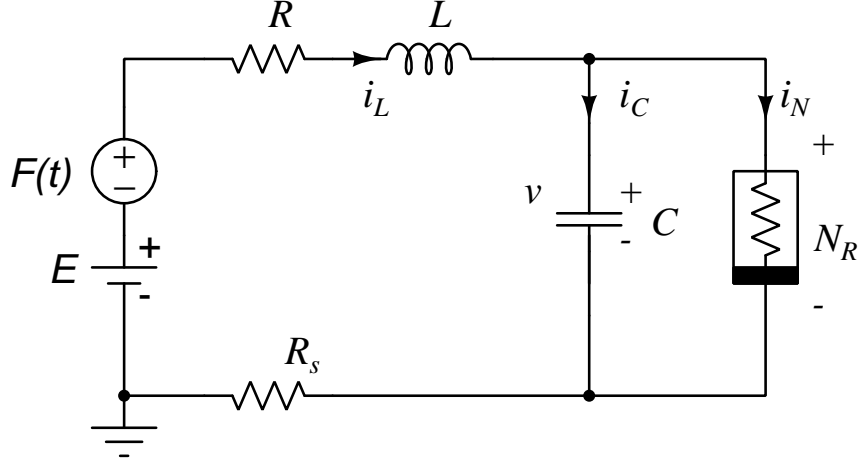


Figure 1: Circuit realization of periodically driven MLC circuit with a DC offset voltage E . Here, N_R is the *Chua's diode*. The parameter values of the other elements are fixed as $L = 18.0 \text{ mH}$, $C = 10.0 \text{ nF}$, $R = 1340 \text{ } \Omega$ and $R_s = 20 \text{ } \Omega$.

the *Chua's diode* as shown in Fig. 2 and is given by

$$g(v) = G_b v + 0.5(G_a - G_b)[|v + B_p| - |v - B_p|], \quad (2a)$$

or in the piecewise-linear form it is given as

$$g(v) = \begin{cases} G_b v + (G_a - G_b) & \text{if } v \geq 1 \\ G_a v & \text{if } |v| \leq 1 \\ G_b v - (G_a - G_b) & \text{if } v \leq -1 \end{cases} \quad (2b)$$

The construction of *Chua's diode* using operational amplifiers (Op-Amps) and its corresponding *Voltage-Current* characteristics is shown in Fig. 2. The parameters of the circuit elements are fixed at $L = 18.0 \text{ mH}$, $C = 10.0 \text{ nF}$, $R = 1340 \text{ } \Omega$, $R_s = 20 \text{ } \Omega$, $G_a = -0.76 \text{ mS}$, $G_b = -0.41 \text{ mS}$ and $B_p = 1.0 \text{ V}$ and the frequency ($\nu = \Omega/2\pi$) of the external forcing source is 8890 Hz . The parameters $F(t)$ and E are taken as control parameters. The dynamical state of the circuit can be kept either in the chaotic or periodic state and the offset voltage E is varied to observe the

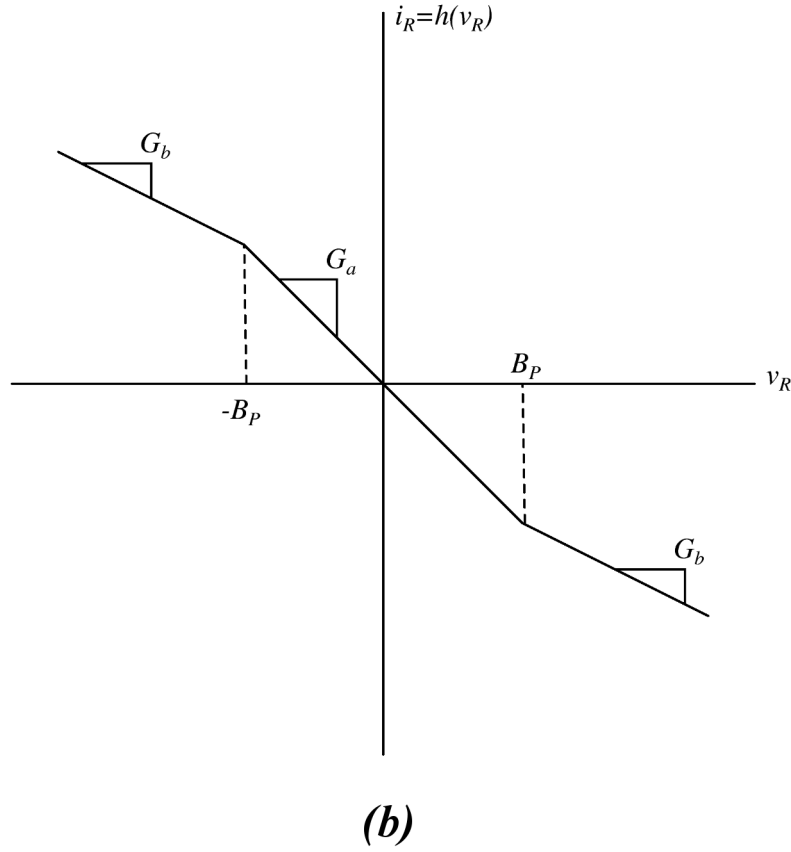
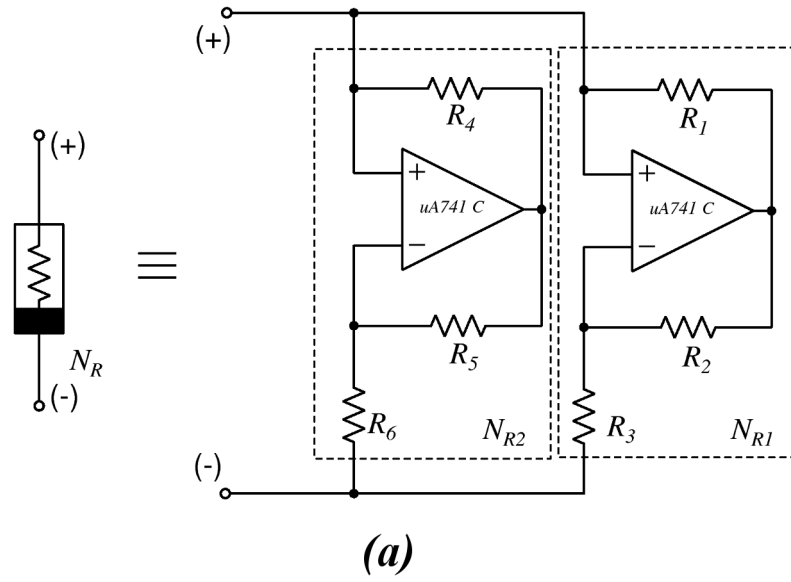


Figure 2: a) Schematic realization of *Chua's* diode N_R using Op-Amps. (b) Voltage-Current characteristics of *Chua's* diode indicating its piecewise-linear nature.

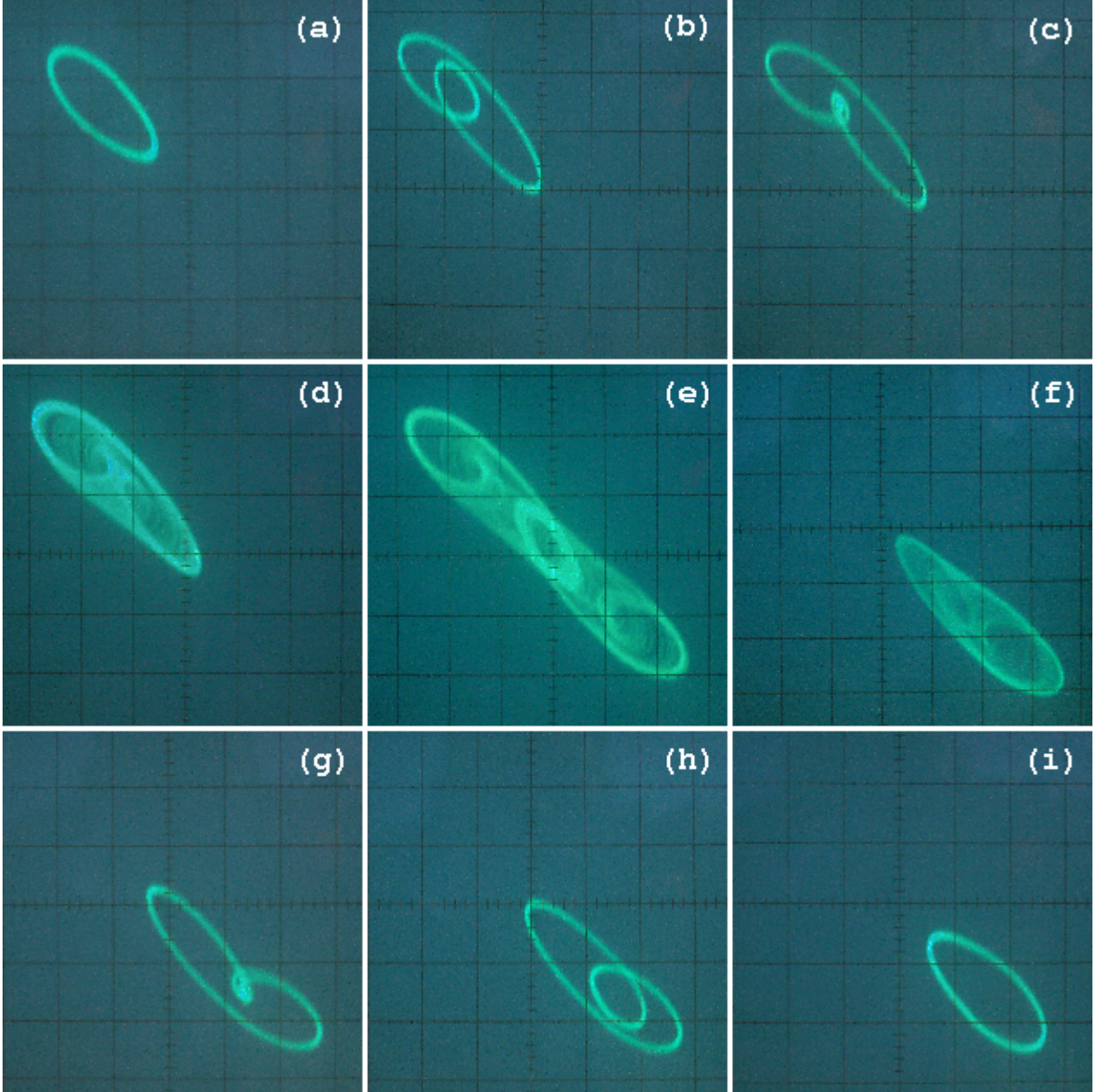


Figure 3: Dynamical hysteresis observed in MLC circuit with variation of offset voltage E . The system is set for one-bane chaotic attractor state for $F = 0.11$ V with $E = 0$. Phase-portraits in the left-half of $v - i_L$ plane: (a) $E = -0.02$ V, period-1T LC (b) $E = -15$ mV, period-2T LC (c) $E = -8.0$ mV, period-4T LC (d) $E = -2.5$ mV, one band chaos and (e) $E = 0.1$ mV, double band chaotic attractor. Phase-portraits in the right-half of $v - i_L$ plane: (f) $E = 2.5$ mV, one band chaos (g) $E = 8.0$ mV, period-4 T LC (h) $E = 15$ mV, period-2T LC (i) $E = 0.02$ V, period-1T LC. LC-Limit Cycle.

changes in the dynamics of the system. Figure 3 shows the experimental dynamics of the *MLC* circuit by varying the offset voltage E with the circuit initially operated at the one-band chaotic attractor state for $F = 0.11$ V when $E = 0$. Hence, in the absence of the DC offset, the system operates in the one-band chaotic attractor state. The DC offset voltage is increased from negative to positive values and the dynamics observed in the $v - i_L$ plane is reported. A period-1 limit cycle is observed for $E = -0.02$ V leading to period-2 and period-4 limit cycles for $E = -15$ mV and $E = -8.0$ mV as shown in Fig. 3(a), 3(b) and 3(c), respectively. Further increase in V leads to an one-band chaotic attractor in the left-half plane for $E = -2.5$ mV followed by a double-band chaotic attractor at $E = 0.1$ mV as shown in Fig. 3(d) and 3(e), respectively. With increase in E , the dynamics of the system jumps to the right-half plane and results in the evolution of an one-band chaotic attractor shown in Fig. 3(g) at $E = 2.5$ mV. Further increase in E indicates a reverse period-doubling sequence represented by the period-4, period-2 and period-1 limit cycles for the values $E = 8.0$ mV, $E = 15$ mV and $E = 0.02$ V as shown in Fig. 3(g), 3(h) and 3(i), respectively. However, when we start from the period-1 limit cycle at the right-half plane, the decrease in E results in the system dynamics indicated by Figs. 3(i), 3(h) and 3(g), 3(f) and gives rise to the double-band chaotic attractor of Fig. 3(e). Further decrease in V results in the jumping of the dynamics to the left-half plane through the evolution of the one-band chaotic attractor shown in Fig. 3(d) followed by the reverse period-doubling sequence of the periodic attractors in the left-half plane. The region of E encompassing the evolution of one-band chaotic attractor in the left-half plane followed by the double-band chaotic attractor leading to the one-band chaotic attractor in the right-half plane when E is increased from negative values and the similar dynamics observed when E is decreased such that the one-band chaotic attractor transits from the right-half plane to the left-half plane through the evolution of the double-band chaotic attractor represents the region of dynamical hysteresis observed in the circuit system.

3 Dynamical hysteresis: Numerical results

In this section, we report the emergence of dynamical hysteresis in MLC circuit through numerical simulation of the normalized circuit equations. Using suitable rescaling factors, the normalized equations obtained from Eq. (1) is written as

$$\dot{x} = y - g(x), \quad (3a)$$

$$\dot{y} = -\sigma y - \beta x + f \sin(\omega t) + c, \quad \left(\cdot = \frac{d}{dt} \right) \quad (3b)$$

where $t = (\tau G/C)$, $\sigma = (\beta + \nu\beta)$, $\beta = (C/LG^2)$, $\nu = GR_s$, $a = G_a/G$, $b = G_b/G$, $f = (F\beta/B_p)$, $\omega = (\Omega C/G)$, $c = (E\beta/B_p)$, $G = 1/R$. The nonlinear function $g(x)$ is written in its normalized form as

$$g(x) = bx + 0.5(b - a)[|x + 1| - |x - 1|] \quad (4a)$$

In piecewise-linear form $g(x)$ is

$$g(x) = \begin{cases} bx + (a - b) & \text{if } x \geq 1 \\ ax & \text{if } |x| \leq 1 \\ bx - (a - b) & \text{if } x \leq -1 \end{cases} \quad (4b)$$

The phenomenon of dynamical hysteresis is studied using the one-parameter bifurcation diagram obtained through numerical simulation of the circuit equations. The normalized system parameters are fixed as $a = -1.02$, $b = -0.55$, $\beta = 1.0$, $\nu = 0.015$, $\omega = 0.75$. Figure 4 shows the one-parameter bifurcation diagram obtained for two different initial conditions and for the existence of the attractors in the left-half plane and right-half plane. The system is initially set at the one-band chaotic attractor state for $f = 0.1104$ when the offset voltage parameter $c = 0$. The period-doubling sequence leading to chaos obtained for the initial condition $(x_0, y_0) = (-0.1, -0.1)$

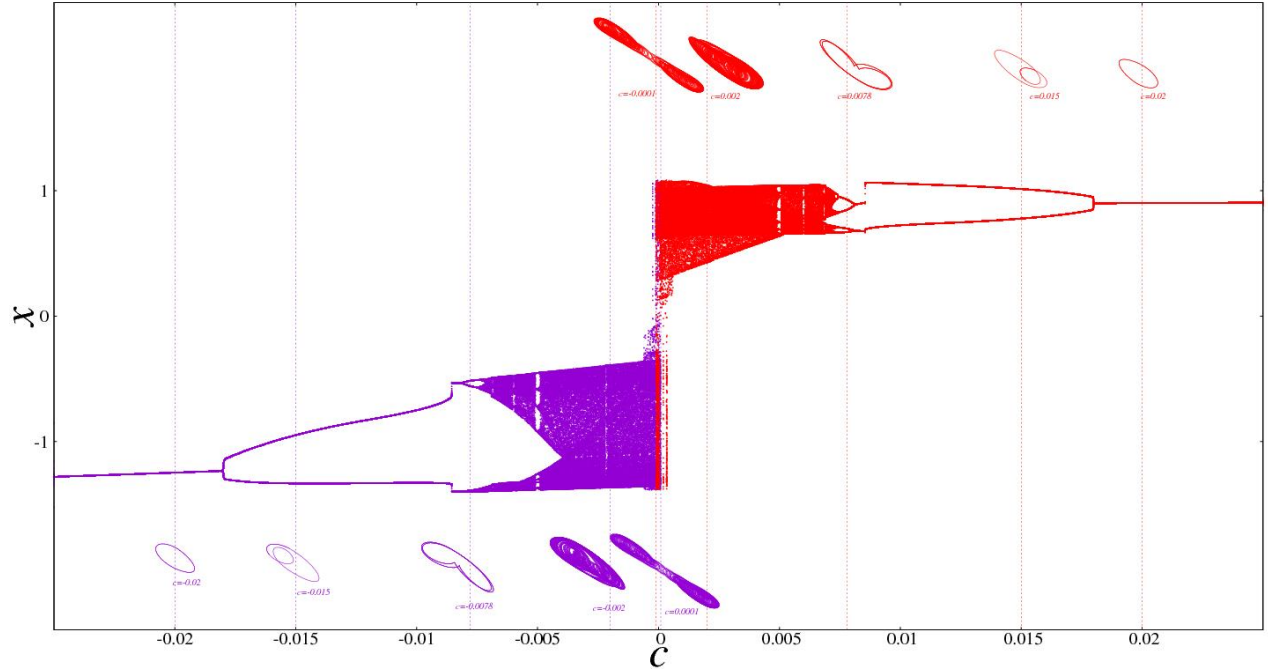


Figure 4: Numerical results: One-parameter bifurcation diagram in the $c - x$ plane obtained in the range $-0.025 < c < 0.002$ for the initial conditions $(x_0, y_0) = (-0.1, -0.1)$ is indicated in violet while the bifurcation diagram in the range $0.025 > c > -0.002$ indicated in red is obtained for the initial condition $(x_0, y_0) = (0.1, -0.1)$. The region of the bifurcation diagram in violet corresponds to the attractor in the LHP while the region in red corresponds to the attractors in the RHP of the phase space. The vertical dashed lines in violet/red indicate the dynamics of the system at that point of c which is also represented by the corresponding colored phase-portraits in the $(x - y)$ plane. The system jumps from the LHP to RHP at $c = 0.002$ in the one-band chaotic state while the dynamics jumps from the RHP to LHP at $c = -0.002$ in the one-band chaotic attractor state. The region of c in the range $-0.002 \leq c \leq 0.002$ indicates the region of dynamical hysteresis.

by sweeping the parameter c in the range $-0.025 < c < 0.002$ is represented in violet while that obtained for the initial condition $(x_0, y_0) = (0.1, -0.1)$ by sweeping the parameter c in the range $0.025 > c > -0.002$ is represented in red. The periodic and the chaotic attractors plotted at their respective positions are indicated by the vertical lines of their respective colors. The values of c in the range $-0.025 < c < 0.002$ represented in violet indicate the attractors in the left-half plane (LHP) and the attractors in the right-half plane (RHP) are indicated in red in the range $0.025 > c > -0.002$. In particular, the system exhibits chaotic attractors in the LHP at the values $c = -0.002$ and $c = 0$ and a double-band chaotic attractor evolves at $c = 0.0001$. At $c = 0.002$, the system jumps to the RHP as a one-band chaotic attractor. Similarly, varying c in the range $0.025 > c > -0.002$ represented in red indicates the existence of attractors in the RHP with one-band and double-band chaotic attractors observed at the values $c = 0.002$ and $c = -0.0001$, respectively. At $c = -0.002$, the system jumps to the LHP as a one-band chaotic attractor. Hence, the parameter range $-0.002 \geq c \geq 0.002$ indicates the emergence and existence of dynamical hysteresis when it is initially operated in the one-band chaotic attractor state. It has to be noted that the system exists in the one-band chaotic attractor state for $c = 0$ and its location in the phase plane corresponds to the dynamical path of operation i.e. either from the LHP or RHP. In the next section, we report the analytical solutions developed for studying dynamical hysteresis in the system.

4 Dynamical hysteresis: Analytical solutions

4.1 Explicit analytical solutions

In this section, we report the explicit analytical solutions developed for the state equations of the MLC circuit with offset voltage and study the hysteresis of the system dynamics using the analytical solutions. The MLC circuit system represented by Eq. (3) is solved for the variables $x(t), y(t)$ in each of the piecewise-linear region and the solutions are matched across the break-point regions for generating the attractors in the phase plane. The analytical solutions for each region is summarized as follows.

4.1.1 D_0 region

In this region, $h(x) = ax$ and the state equations are written as

$$\frac{dx}{dt} = y - ax, \quad (5a)$$

$$\frac{dy}{dt} = -\beta y - \nu\beta y - \beta x + f \sin(\omega t) + c, \quad (5b)$$

The Jacobian matrix determining the stability of the fixed point $p_0 = (0, 0)$ in this region is

$$J_0 = \begin{pmatrix} -a & 1 \\ -\beta & -(\beta + \nu\beta) \end{pmatrix}, \quad (6)$$

Equation (5) written as a second-order differential equation is given as

$$\ddot{y} + A_1 \dot{y} + B_1 y = \Delta_1 + af \sin(\omega t) + f\omega \cos(\omega t), \quad (7)$$

where $A_1 = \beta + \nu\beta + a$, $B = \beta + a(\beta + \nu\beta)$ and $\Delta = ac$. For the given values of the system parameters, the roots of Eq. (7) $m_{1,2} = \frac{-A_1}{2} \pm \frac{\sqrt{A_1^2 - 4B_1}}{2}$ are real and distinct and the state variables are obtained as

$$y(t) = C_1 e^{m_1 t} + C_2 e^{m_2 t} + E_1 + E_2 \sin(\omega t) + E_3 \cos(\omega t), \quad (8a)$$

$$x(t) = \frac{1}{\beta} (-(\beta + \nu\beta)y - \dot{y} + c + f \sin(\omega t)), \quad (8b)$$

where, the constants E_1, E_2, E_3, C_1, C_2 are

$$E_1 = \frac{\Delta}{B_1} \quad (9a)$$

$$E_2 = \frac{f\omega^2(A-a) + afB}{A^2\omega^2 + (B-\omega^2)^2} \quad (9b)$$

$$E_3 = -\frac{f\omega(Aa + \omega^2 - B)}{A^2\omega^2 + (B-\omega^2)^2} \quad (9c)$$

$$C_1 = \frac{e^{-m_1 t_0}}{m_1 - m_2} \{(-(\beta + \nu\beta + m_2)y_0 - \beta x_0 + c + m_2 E_1) - (\omega E_2 - m_2 E_3) \cos \omega t_0 + (\omega E_3 + m_2 E_2 + f) \sin \omega t_0\} \quad (9d)$$

$$C_2 = \frac{e^{-m_2 t_0}}{m_2 - m_1} \{(-(\beta + \nu\beta + m_1)y_0 - \beta x_0 + c + m_1 E_1) - (\omega E_2 - m_1 E_3) \cos \omega t_0 + (\omega E_3 + m_1 E_2 + f) \sin \omega t_0\} \quad (9e)$$

4.1.2 D_{+1} region

In D_{+1} region, $h(x) = bx + (a - b)$ and the state equations are written as

$$\frac{dx}{dt} = y - bx - (a - b), \quad (10a)$$

$$\frac{dy}{dt} = -\beta y - \nu\beta y - \beta x + f \sin(\omega t) + c, \quad (10b)$$

The Jacobian matrix determining the stability of the fixed point $p_1 = (\frac{(\beta+\nu\beta)(b-a)}{b(\beta+\nu\beta)+\beta}, \frac{\beta(a-b)}{b(\beta+\nu\beta)+\beta})$ in this region is

$$J_0 = \begin{pmatrix} -b & 1 \\ -\beta & -(\beta + \nu\beta) \end{pmatrix}, \quad (11)$$

Equation (10) can be written as a second-order differential equation in terms of the variable y as

$$\ddot{y} + A_2 \dot{y} + C_2 y = \Delta_2 + bf \sin(\omega t) + f\omega \cos(\omega t), \quad (12)$$

where $A_2 = \beta + \nu\beta + b$, $B_2 = \beta + b(\beta + \nu\beta)$ and $\Delta_2 = bc + \beta(a - b)$. For the given values of the system parameters, the roots of Eq. (12) $m_{3,4} = u \pm iv$, where, $u = \frac{-A_2}{2}$, $v = \frac{\sqrt{4B_2 - A_2^2}}{2}$ are a pair of complex conjugates and the state variables are obtained as

$$y(t) = e^{ut}(C_3 \cos vt + C_4 \sin vt) + E_4 + E_5 \sin(\omega t) + E_6 \cos(\omega t), \quad (13a)$$

$$x(t) = \frac{1}{\beta}(-(\beta + \nu\beta)y - \dot{y} + c + f \sin(\omega t)), \quad (13b)$$

The constants E_4, E_5, E_6 are the same as E_1, E_2, E_3 of Eq. (9) except the constants Δ_1, a are replaced with Δ_2, b , respectively. The constants of the complementary function C_3, C_4 are

$$\begin{aligned} C_3 &= \frac{e^{-ut_0}}{v} \{ ((\beta + \nu\beta + u)y_0 + \beta x_0 - c) \sin vt_0 + (vy_0 - vE_4) \cos vt_0 - uE_4 \sin vt_0 \\ &\quad + ((\omega E_5 - uE_6) \sin vt_0 - vE_6 \cos vt_0) \cos \omega t_0 \\ &\quad - ((\omega E_6 + uE_5 + f) \sin vt_0 + vE_5 \cos vt_0) \sin \omega t_0 \} \\ C_4 &= \frac{e^{-ut_0}}{v} \{ (c - (\beta + \nu\beta + u)y_0 - \beta x_0) \cos vt_0 + (vy_0 - vE_4) \sin vt_0 + uE_4 \cos vt_0 \\ &\quad - ((\omega E_5 - uE_6) \cos vt_0 + vE_6 \sin vt_0) \cos \omega t_0 \\ &\quad + ((\omega E_6 + uE_5 + f) \cos vt_0 - vE_5 \sin vt_0) \sin \omega t_0 \} \end{aligned}$$

4.1.3 D_{-1} region

In this region, $h(x) = bx - (a - b)$ and the state equations are written as

$$\frac{dx}{dt} = y - bx + (a - b), \quad (14a)$$

$$\frac{dy}{dt} = -\beta y - \nu\beta y - \beta x + f \sin(\omega t) + c, \quad (14b)$$

The Jacobian matrix determining the stability of the fixed point $p_2 = (\frac{(\beta+\nu\beta)(a-b)}{b(\beta+\nu\beta)+\beta}, \frac{\beta(b-a)}{b(\beta+\nu\beta)+\beta})$ in this region is obtained from Eq. (11). The state equation written in terms of the variable y is

$$\ddot{y} + A_3\dot{y} + C_3y = \Delta_3 + bf\sin(\omega t) + f\omega\cos(\omega t), \quad (15)$$

where $A_3 = \beta + \nu\beta + b$, $B_3 = \beta + b(\beta + \nu\beta)$ and $\Delta_3 = bc - \beta(a - b)$. The roots of eq. (15) are a pair of complex conjugates given as $m_{3,4} = u \pm iv$, where, $u = \frac{-A_3}{2}$, $v = \frac{\sqrt{4B_3 - A_3^2}}{2}$ and the state variables are obtained as

$$y(t) = e^{ut}(C_5 \cos vt + C_6 \sin vt) + E_7 + E_8 \sin(\omega t) + E_9 \cos(\omega t), \quad (16a)$$

$$x(t) = \frac{1}{\beta}(-(\beta + \nu\beta)y - \dot{y} + c + f \sin(\omega t)), \quad (16b)$$

The constants E_7, E_8, E_9, C_5, C_6 are the same as E_4, E_5, E_6, C_3, C_4 of D_{+1} region except that Δ_2, a is replaced with Δ_3 . The analytical solutions are used to generate the trajectories in the $(x - y)$ phase plane of the system by varying a control parameter of the system for the fixed values of other parameters.

The emergence of dynamical hysteresis in the system observed using the explicit analytical solutions briefed above is depicted in Fig. 5. The *MLC* circuit is initially set for the one-band chaotic attractor state at $c = 0$. The one-band chaotic attractor is so chosen such that it exists at the edge of the one-band chaotic state. The parameter values are kept at the values $a = -1.02, b = -0.55, \beta = 1.0, \nu = 0.015, f = 0.1105, \omega = 0.75$. Increasing c value from $c = -0.02$ with the system operating initially ($c = 0$) at the one-band chaotic attractor state around the fixed point p_2 in clockwise direction in the LHP for the initial condition $x_0, y_0 = -0.1, -0.1$ yields the dynamical path *ABCDEFJIHG*. The violet colored region indicates the dynamics of the existing in the LHP while the red colored corresponds to the dynamics in the RHP. The phase-portraits existing in the LHP corresponding to the points of the dynamical path is presented near each point. The different dynamical behaviors of the system at each of the points is briefed in Table 1. From Fig.

5 it is observed that the one-band chaotic attractor existing in the LHP (E) existing around the fixed point p_2 at $c = 0$ jumps to the RHP as an one-band chaotic attractor (J) evolving around the fixed point p_1 in the clockwise direction at $c = 0.0025$ through the evolution of the double-band chaotic attractor (F) at $c = 0.0001$ and the system exhibits reverse period-doubling sequence with the attractors existing in the RHP represented by attractors and path in red. Similarly, decreasing c from $c = 0.02$ with the system operating initially ($c = 0$) at the one-band chaotic state in the RHP around the fixed point p_1 yields the dynamical path $GHIJKLDCBA$. The transition of the one-band chaotic attractor state existing around p_1 in the RHP at $c = 0$ to an attractor existing around p_2 in the LHP at the value $c = -0.0025$ (D) is observed through the evolution of a double-band chaotic attractor state at $c = -0.0001$ (L). The intersection of the paths $ABCDEFJIHG$ and $GHIJKLDCBA$ yields the region of dynamical hysteresis represented by $DEFJKL$ which is in confirmation with the dynamical region represented in the numerical simulation results shown in Fig. 4.

The dynamical hysteresis observed in the *MLC* circuit with the system initially operating in the double-band chaotic attractor state is depicted in Fig. 6. The circuit is operated at the double-band chaotic state for $c = 0$ and the other parameters are set as $a = -1.02, b = -0.55, \beta = 1.0, \nu = 0.015, f = 0.13, \omega = 0.75$. The phenomenon of dynamical hysteresis is observed as the parameter c is increased in the range $-0.03 \leq c \leq 0.03$. The system exhibiting a period-T limit cycle attractor at $c = -0.03$ about the fixed point p_2 evolves into a period-2T limit cycle at $c = -0.025$ before settling down into an one-band chaotic attractor at $c = -0.01$ as shown in Figs. 6(a), 6(b) and 6(c), respectively. Increasing the value of c results in a double-band chaotic attractor at $c = 0$ as shown in Fig. 6(d). Further increase in c results in a one-band chaotic attractor evolving around the fixed point p_2 in the RHP at $c = 0.01$ leading to a period-2T attractor at $c = 0.025$ as shown in Figs. 6(e) and 6(f), respectively. The system finally settles down to a period-T limit cycle attractor at $c = 0.03$ as observed in Fig. 6(g). The dynamical hysteresis behavior is also observed when the parameter is decreased from 0.03 to -0.03 . In either case, the hopping of the attractors around the fixed points p_1 to p_2 and *vice versa* about the double-band chaotic attractor state for equal and

Dynamical Point	c	Dynamical state	LHP/RHP
A	-0.02	period-1T LC	LHP
B	-0.015	period-1T LC	LHP
C	-0.0078	period-4T LC	LHP
D	-0.0025	One-band chaos	LHP
E	0.0	One-band chaos	LHP
F	0.0001	Double-band chaos	Both
G	0.02	period-1T LC	RHP
H	0.015	period-1T LC	RHP
I	0.0078	period-4T LC	RHP
J	0.0025	One-band chaos	RHP
K	0.0	One-band chaos	RHP
L	-0.0001	Double-band chaos	Both

Table 1: Dynamics of the MLC system at the dynamical points specified in Fig. 5. LC-Limit Cycle.

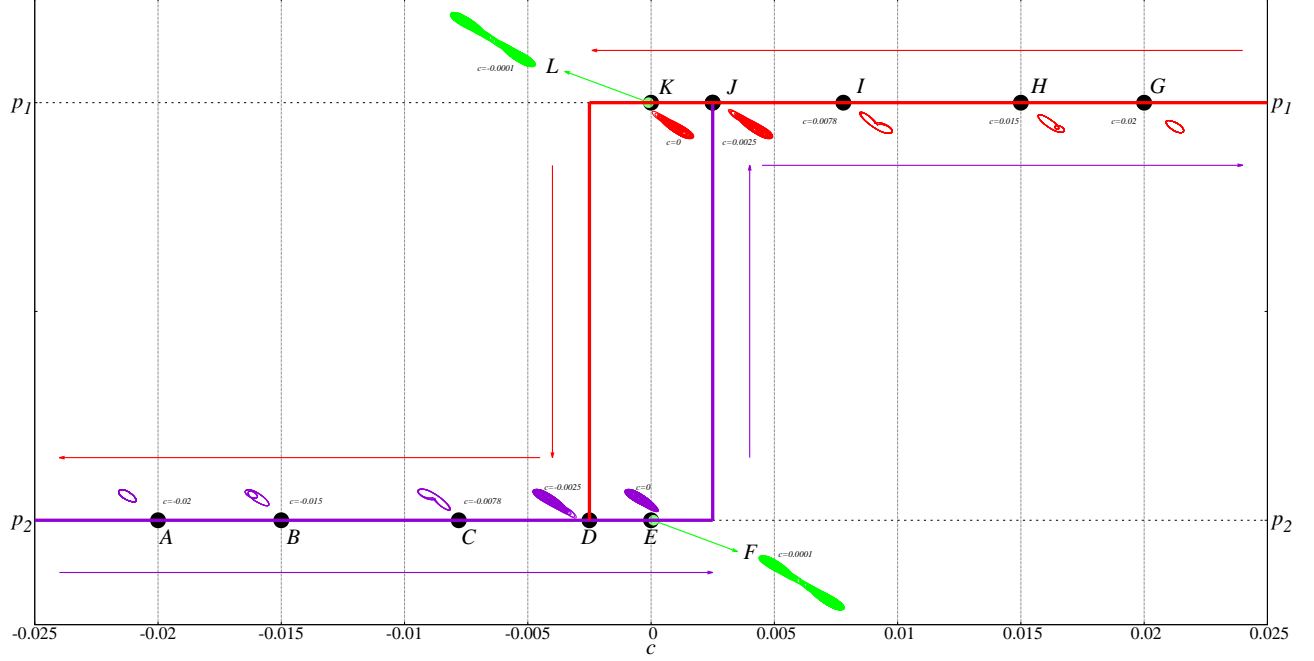


Figure 5: Analytical results: Dynamical hysteresis observed in *MLC* circuit through explicit analytical solutions. The system is initially operated in the one-band chaotic attractor state ($c = 0$) existing in the left-half or right-half plane. The increase of the parameter c from in the range $-0.02 \leq c \leq 0.02$ with the attractor fixed in the left-half plane ($c = 0$) yields the dynamical path *ABCDEFJIHG*. The chaotic attractors in the $x - y$ plane is plotted adjacent to each of the dynamical path points. Conversely, the dynamical path *GHIJKLDCBA* is observed when the attractor is initially set at the right-half plane ($c = 0$) and for c varying in the range $0.02 \geq c \geq -0.02$. The intersection of these dynamical paths reveals the existence of the dynamical hysteresis represented by the path *DEFJKL*. The jumping of the attractor from the left-half to right-half plane and vice-versa occurs through the evolution of the double-band chaotic attractor state.

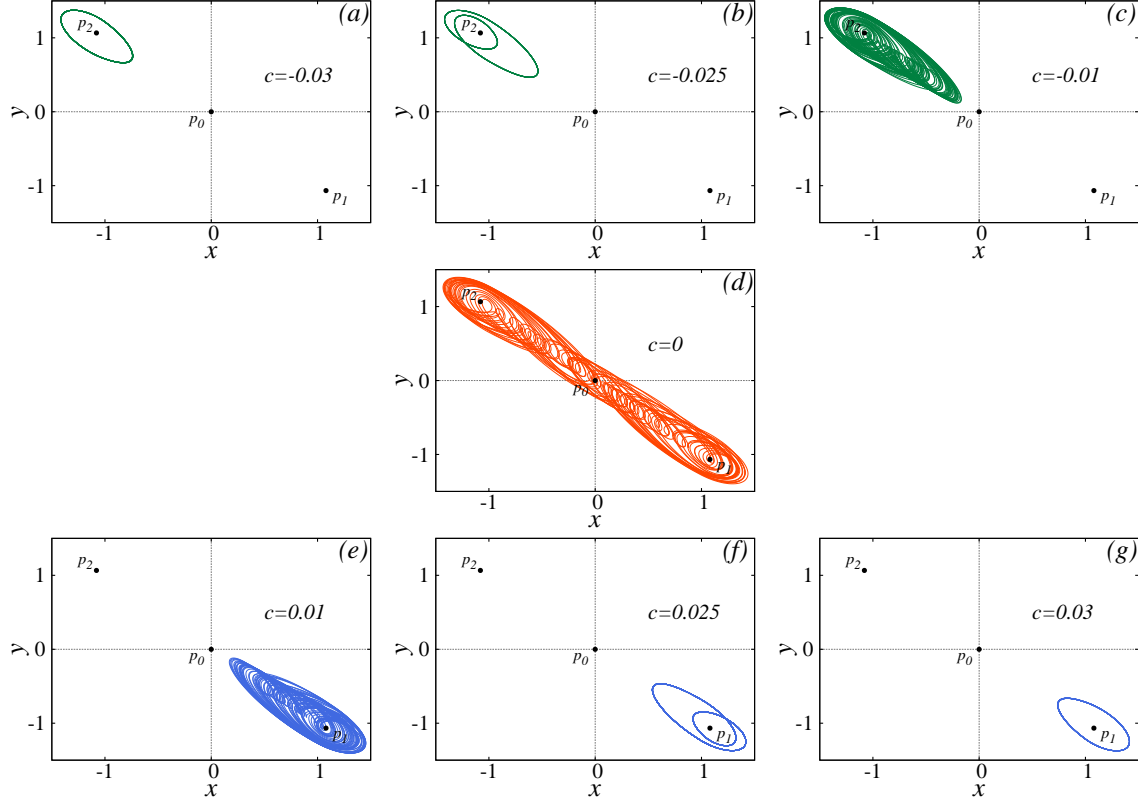


Figure 6: Analytical results indicating the phenomena of dynamical hysteresis in MLC circuit for the offset voltage factor c as the control parameter. (a) Period-T attractor for $c = -0.03$, (b) Period-2T attractor for $c = -0.025$ and (c) one-and chaotic attractor for $c = -0.01$ obtained in the LHP around the fixed point p_1 ; (d) double-band chaotic attractor for $c = 0$; (e) one-and chaotic attractor for $c = 0.01$, (f) Period-2T attractor for $c = 0.025$ and (g) Period-T attractor for $c = 0.3$ obtained in the RHP around the fixed point p_2 .

opposite values of c indicating the phenomenon of dynamical hysteresis is observed.

5 Conclusion

The emergence of dynamical hysteresis in the *Murali-Lakshmanan-Chua* (MLC) circuit is reported in this paper. The observation of hysteresis in the dynamics of the third-order *Chua's* circuit has been reported recently. The MLC circuit being a second-order non-autonomous circuit which exhibits nearly all the complex phenomena observed in the *Chua's* circuit. The present work reveals the evolution of dynamical hysteresis in the MLC circuit due to the inclusion of an offset voltage parameter in the circuit. The MLC circuit initially set to operate at the one-band chaotic state in the absence of the offset voltage parameter jumps from one-half plane to another and vice versa through the evolution of a double-band chaotic attractor as the offset voltage parameter is varied. The existence of hysteresis over a certain region of the offset voltage parameter encompassing the initial state is observed and reported. The phenomenon of dynamical hysteresis observed by electronic circuit experiments is validated through numerical and analytical results. The circuit can be set to operate at different initial dynamical states to study the emergence of dynamical hysteresis in different regions with different dynamical behaviors.

Acknowledgement

The authors are grateful to Dr.K. Murali, Professor, Department of Physics, Anna University, Chennai, India for his valuable suggestions and discussions.

References

- [1] Iacyel Gomes, Wojciech Korneta, Stavros G. Stavrinos, Rodrigo Picos, and Leon O. Chua. Experimental observation of chaotic hysteresis in chua's circuit driven by slow voltage forcing. *Chaos, Solitons & Fractals*, 166:112927, 2023.

- [2] T. Matsumoto. A chaotic attractor from chua's circuit. *IEEE Transactions on Circuits and Systems*, 31(12):1055–1058, December 1984.
- [3] T. Matsumoto, L. O. Chua, and M. Komuro. The double scroll. *IEEE Transactions on Circuits and Systems*, 32(8):797–818, August 1985.
- [4] L. O. Chua, M. Komuro, and T. Matsumoto. The double scroll family. *IEEE Transactions on Circuits and Systems*, 33(11):1072–1118, November 1986.
- [5] M. P. Kennedy. Robust op amp realization of Chua's circuit. *Frequenz*, 46(3):66–80, 1992.
- [6] K. Murali and M. Lakshmanan. Bifurcation and chaos of the sinusoidally - driven Chua's circuit. *International Journal of Bifurcation and Chaos*, 01(02):369–384, 1991.
- [7] K. Murali and M. Lakshmanan. Effect of sinusoidal excitation on the chua's circuit. *IEEE Transactions on Circuits and Systems I: Fundamental Theory and Applications*, 39(4):264–270, 1992.
- [8] Z. Zhu and Z. Liu. Strange nonchaotic attractors of chua's circuit with quasiperiodic excitation. *International Journal of Bifurcation and Chaos*, 07(01):227–238, 1997.
- [9] K. Thamilmaran, M. Lakshmanan, and A. Venkatesan. Hyperchaos in a modified canonical Chua's circuit. *International Journal of Bifurcation and Chaos*, 14(01):221–243, 2004.
- [10] K. Srinivasan, K. Thamilmaran, and A. Venkatesan. Classification of bifurcations and chaos in chua's circuit with effect of different periodic forces. *International Journal of Bifurcation and Chaos*, 19(06):1951–1973, 2009.
- [11] K. Srinivasan, G. Sivaganesh, T. Fonzin Fozin, and I. Raja Mohamed. Analytical studies on complete, lag and anticipation synchronization in cascaded circuits with numerical and experimental confirmation. *AEU - International Journal of Electronics and Communications*, 159:154491, 2023.

- [12] G. Sivaganesh and K. Srinivasan. Theoretical investigations on the multistability, quasiperiodicity and synchronization of the driven chua's circuit. *Circuits Systems and Signal Processing*, 2023.
- [13] L. Fortuna, M. Frasca, and A. Rizzo. Frequency hysteresis phenomena in the frequency switched chua's circuit. In *ISCAS 2001. The 2001 IEEE International Symposium on Circuits and Systems (Cat. No.01CH37196)*, volume 3, pages 277–280 vol. 2, 2001.
- [14] J.-P. Françoise and C. Piquet. Hysteresis dynamics, bursting oscillations and evolution to chaotic regimes. *Acta Biotheoretica*, 53:381–32, 2005.
- [15] P. Vadasz. Chaotic dynamics and hysteresis in thermal convection. *Proceedings of the Institution of Mechanical Engineers, Part C: Journal of Mechanical Engineering Science*, 220(3):309–323, 2006.
- [16] S. K. Dana, S. Chakraborty, and G. Ananthakrishnan. Homoclinic bifurcation in chua's circuit. *Pramana*, 64:443–454, 2005.
- [17] Satyabrata Chakraborty and Syamal Kumar Dana. Shil'nikov chaos and mixed-mode oscillation in chua circuit. *Chaos: An Interdisciplinary Journal of Nonlinear Science*, 20(2):023107, 2010.
- [18] Weiqing Liu, Yin Guo, Min Lu, and Chaofei Liu. Chaos attractor compressing and expanding in chua circuit driven by direct current voltage. In *2010 Third International Symposium on Information Science and Engineering*, pages 446–450, 2010.
- [19] Mo Chen, Ankai Wang, Chao Wang, Huagan Wu, and Bocheng Bao. Dc-offset-induced hidden and asymmetric dynamics in memristive chua's circuit. *Chaos, Solitons & Fractals*, 160:112192, 2022.

- [20] K. Murali, M. Lakshmanan, and L. O. Chua. The simplest dissipative nonautonomous chaotic circuit. *IEEE Transactions on Circuits and Systems-I: Fundamental Theory and Applications*, 41:462–463, 1994.
- [21] M.Lakshmanan and K.Murali. Experimental chaos from non-autonomous electronic circuits. *Phil. Trans.: Physical Sciences and Engineering: Chaotic Behaviour in Electronic Circuits*, 353:33–46, 1995.
- [22] M. Lakshmanan and K. Murali. *Chaos in Nonlinear Oscillators: Controlling and Synchronization*. World Scientific Series on Nonlinear Science, Singapore, 1996.
- [23] K.Murali and M.Lakshmanan. Controlling and synchronization of chaos in the simplest dissipative non-autonomous circuit. *International Journal of Bifurcation and Chaos*, 5:563–571, 1995.
- [24] A. Venkatesan, K. Murali, and M. Lakshmanan. Birth of strange nonchaotic attractors through type iii intermittency. *Physics Letters A*, 259(3):246–253, 1999.
- [25] G. Sivaganesan, A. Arulgnanam, and A.N. Seethalakshmi. Generalized analytical solutions and experimental confirmation of complete synchronization in a class of mutually coupled simple nonlinear electronic circuits. *Chaos, Solitons & Fractals*, 113:294 – 307, 2018.
- [26] G. Sivaganesan, A. Arulgnanam, and A. N. Seethalakshmi. A complete analytical study on the dynamics of simple chaotic systems. *Pramana*, 92:42, 2019.
- [27] K. Murali, Sudeshna Sinha, Vivek Kohar, Behnam Kia, and William L. Ditto. Chaotic attractor hopping yields logic operations. *PLOS ONE*, 13(12):1–17, 12 2018.
- [28] Dongping Wang, Hui Zhao, and Juebang Yu. Chaos in memristor based murali-lakshmanan-chua circuit. In *2009 International Conference on Communications, Circuits and Systems*, pages 958–960, 2009.

- [29] A. Ishaq Ahamed and M. Lakshmanan. Nonsmooth bifurcations, transient hyperchaos and hyperchaotic beats in a memristive murali–lakshmanan–chua circuit. *International Journal of Bifurcation and Chaos*, 23(06):1350098, 2013.
- [30] A. Ishaq Ahamed and M. Lakshmanan. Sliding bifurcations in the memristive murali–lakshmanan–chua circuit and the memristive driven chua oscillator. *International Journal of Bifurcation and Chaos*, 30(14):2050214, 2020.
- [31] G. Sivaganesh, K. Srinivasan, T. Fozin Fozin, and I. Raja Mohamed. Energy computation and multistability in a class of second-order chaotic systems with simple nonlinearities: numerical, experimental and analytical results. *Physica Scripta*, 98(1):015226, dec 2022.